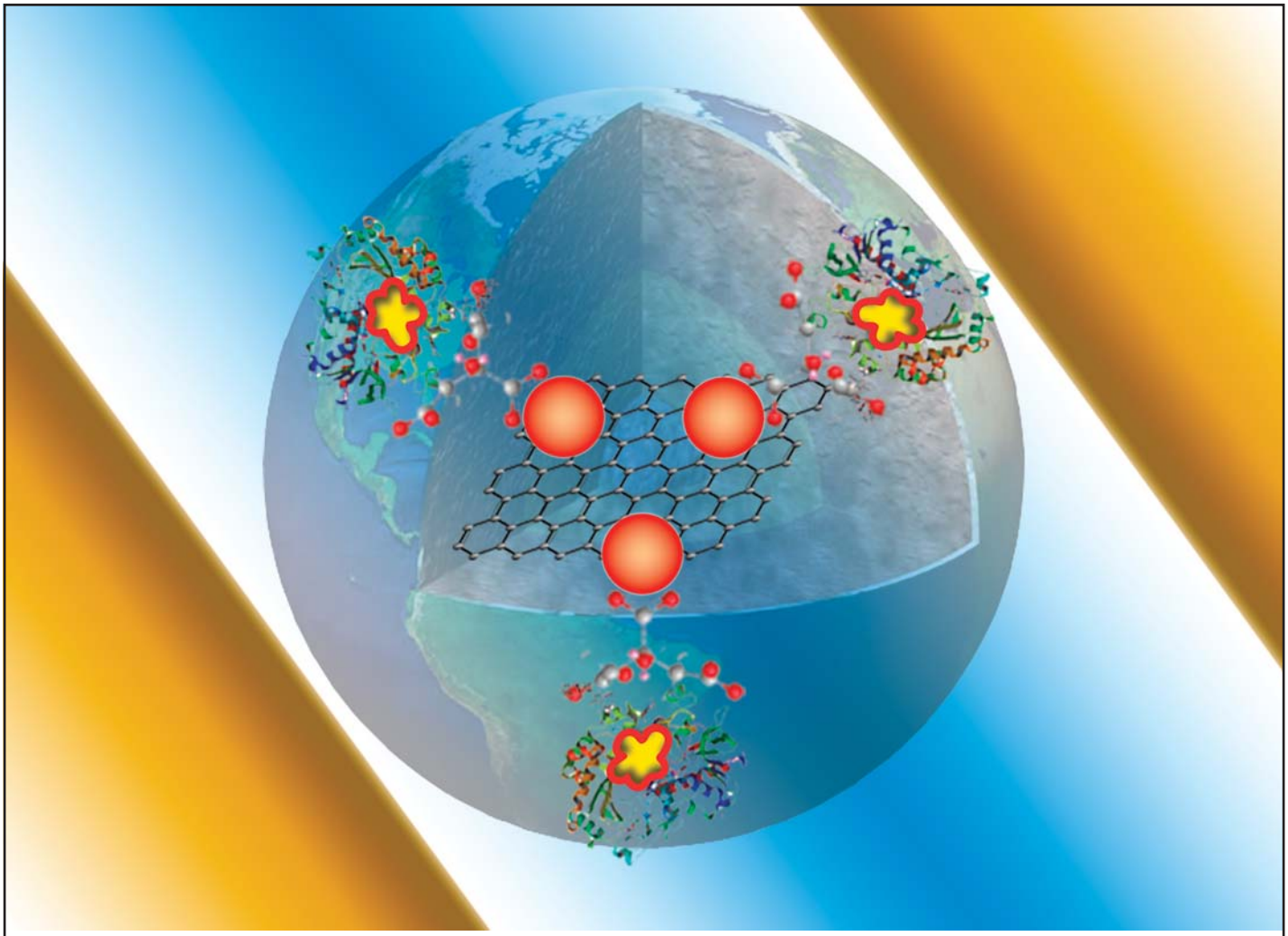

Highlighting research results from Key Laboratory of Analytical Chemistry for Life Science (Ministry of Education of China), School of Chemistry and Chemical Engineering, Nanjing University, P. R. China.

Title: Fabrication of gold nanoparticles on bilayer graphene for glucose electrochemical biosensing

The hydrophilic and carboxyl group functionalized graphene-gold nanoparticles hybrid has been *in situ* synthesized. Glucose oxidase was successfully bound to the surface of the hybrid for fabricating a novel model of a glucose biosensor. Blood sugar concentrations in human serum samples measured by the glucose biosensor were in good agreement with the values provided by Nanjing University hospital. Three constructed biosensors showed good stability, and all of them retained 80% of their initial signals when they were stored at 4 °C after four months.

As featured in:

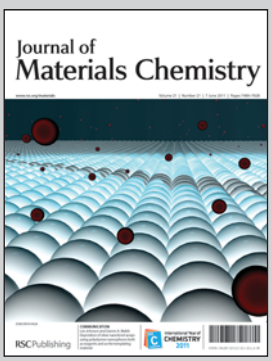

See Y. Chen *et al.*,
J. Mater. Chem., 2011, **21**, 7604.

RSC Publishing

www.rsc.org/materials

Registered Charity Number 207890

Journal of Materials Chemistry

Dynamic Article Links

Cite this: J. Mater. Chem., 2011, 21, 7604

www.rsc.org/materials

PAPER

Fabrication of gold nanoparticles on bilayer graphene for glucose electrochemical biosensing

Yun Chen,[a] Yang Li,[a] Dong Sun,[a] Danbi Tian,[b] Jianrong Zhang*[a] and Jun-Jie Zhu*[a]

Received 20th January 2011, Accepted 11th March 2011
DOI: 10.1039/c1jm10293a

The hydrophilic and carboxyl group functionalized graphene–gold nanoparticles (AuNPs) hybrid has been synthesized *in situ*. AuNPs can be scattered well on the graphene bilayer, and the loading amount of AuNPs can be controlled. Glucose oxidase (GOD) was successfully bound to the surface of the hybrid through a condensation reaction between terminal amino groups on the lysine residues of GOD and carboxyl groups on the AuNPs. The hybrid provided a suitable microenvironment for GOD to retain its biological activity. The direct and reversible electron transfer process between GOD and the hybrid electrode was realized without any supporting film or electron mediator. A novel model of the glucose biosensor based on the hybrid electrode was fabricated. Blood sugar concentrations measured in human serum samples by the glucose biosensor were in good agreement with the values provided by the Nanjing University hospital, and the average relative standard deviation was 3.2% for six successive measurements. Three constructed biosensors showed good stability, and all of them retained 80% of their initial signals after they were stored at 4 °C for four months. It is promising that the model of the glucose biosensor can be used as an effective candidate for the detection of blood sugar concentration in clinical diagnoses.

1. Introduction

Graphene is a single-atom-thick sheet of carbon atoms densely packed into a honeycomb two-dimensional lattice.[1] Because of its fascinating electronic transfer at room temperature,[2] extremely high specific surface area, and preponderance of exposed edge planes to greatly increase charge storage,[3] graphene has attracted extensive attention in electrochemical studies.[4] Recently, the functionalization of graphene has been considered to be important for improving its applications.[5] Many materials such as gold,[6] platinum,[7] palladium,[8] tin oxide,[9] titanium dioxide,[10] latex,[6c] and carbon nanotubes[11] were used to fabricate the functional graphene compositions. Because AuNPs could provide a suitable microenvironment for biomolecule immobilization[4c] and facilitate electron transfer between the immobilized protein and AuNPs,[12] they have been widely applied in immunosensors,[13] biosensors,[14] and in the detection of proteins, bacteria and cells.[15] It is expected that a hybrid composed of graphene and AuNPs could become a novel functional material for application in electrochemistry. Until now, two main methods have been selected to fabricate graphene–AuNPs hybrids. One is using intermedia,[6c–6h] such as bovine serum albumin, for the linkage of AuNPs and graphene to form graphene–media–AuNPs hybrids. The disadvantage of the method is poor conductivity of the hybrid because of the barrier of nonconducting media between the graphene and the AuNPs. In order to overcome this, *in situ* growth of AuNPs on graphene[6a–6b] has been presented. However, the *in situ* growth method has three main limitations:[6c] (1) It lacks good control over the reaction process; (2) The resulting graphene–AuNPs hybrid is mostly in the form of precipitate and not suitable for applications requiring well-dispersed materials; (3) It is still challenging to realize the assembly of homogeneous AuNPs on a single graphene nanosheet without "glue".

Herein, AuNPs were reduced *in situ* onto the surface of graphene in the presence of sodium citrate. By changing the mass ratio of graphene and $HAuCl_4$, the loading amount of AuNPs on the graphene surface was controlled, and the size of the AuNPs was homogeneous. Due to the hydrophilic property of sodium citrate binding on AuNPs, the hybrid was easy to disperse in water and could be kept stable only by mild shaking. To the best of our knowledge, there is no literature reporting the fabrication of the hydrophilic and carboxyl group functionalized graphene–AuNPs hybrid by an *in situ* method. GOD was successfully bound to the surface of the hybrid through a condensation reaction between terminal amino groups on lysine residues of GOD and carboxyl groups on the AuNPs. The direct and reversible electron transfer between GOD and the hybrid

[a]*Key Laboratory of Analytical Chemistry for Life Science (Ministry of Education of China), School of Chemistry and Chemical Engineering, Nanjing University, Nanjing, 210093, P. R. China. E-mail: jrzhang@nju.edu.cn; Fax: +86 25 83594976; Tel: +86 25 83686130; jjzhu@nju.edu.cn*
[b]*College of Science, Nanjing University of Technology, Nanjing, 210009, P. R. China*

electrode was observed. The glucose concentration in human serum samples were tested by the electrochemical biosensor, and the results were consistent with the measurements performed at the Nanjing University hospital.

2. Experimental

2.1 Preparation of the graphene–AuNPs hybrid

Scheme 1 displays the strategy for the preparation of the graphene–AuNPs hybrid. The synthesis of the graphene–AuNPs hybrid can be separated into three steps: Firstly, a graphene colloid was synthesized according to the reference with a mild modification.[16] The slight excess of N_2H_4 existed in the colloid and the zeta potential of graphene was −55 mV. The concentration of graphene was determined by UV-Vis spectroscopy and further determined by a weight loss method. Then, the stoichiometric $HAuCl_4$ was added into the graphene colloid. The gold nuclei can be formed on the graphene surface from the spontaneous reduction of Au^{3+} in the presence of N_2H_4. The mechanism is discussed in the Results and discussion section. Finally, the gold nuclei grew by the reduction of sodium citrate to obtain the graphene–AuNPs hybrid. The optimal condition for the synthesis of the graphene–AuNPs hybrid was as follows: 500 μL of 1% (wt. %) $HAuCl_4$ and 1 mL of 0.1 M freshly prepared sodium citrate added dropwise into 5 mL of 0.7 mg mL^{-1} graphene colloid solution, respectively. Then the solution was stirred at 60 °C for 2 h. The precipitation formed dispersed in water and the homogeneous solution was stable for 1 h. For morphology analysis, the precipitation was collected by centrifugation and rinsed with ultrapure water.

2.2 Material characterization

Zeta potential analysis was performed with a Zetasizer Nano-Z Zeta Potential Analyzer. X-Ray diffraction (XRD) measurements were measured by a Shimadzu XD-3A X-Ray powder diffractometer. The FT-IR spectra of the samples were obtained on a Bruker Vector 22 spectrophotometer. UV-Vis absorption spectra were recorded using a Shimadzu spectrophotometer. Atomic force microscope (AFM) images were performed in tapping mode using an Agilent 5500. Field emission scanning electron microscopy (FESEM) images and high resolution transmission electron microscopy (HRTEM) images were measured by a HITACHI S4800 and a JEOL 2010, respectively. Inductively coupled plasma atomic emission spectroscopy (ICP-AES) was recorded using a J-A1100. Electrochemical measurements were performed on a CHI 660B workstation with a traditional three-electrode system including a Pt wire electrode as the counter electrode, a saturated calomel electrode (SCE) as the reference electrode, and the glass carbon (GC) electrodes (d = 3 mm) as the working electrodes.

2.3 Fabrication of the model of the amperometric glucose biosensor

Scheme 2 shows the strategy of constructing the model of the glucose electrochemical biosensor. The whole process can be divided into three sections. First of all, GC electrodes were carefully polished by 1.0, 0.3, and 0.05 μm alumina powder respectively to a mirror finish, then sonicated in ethanol and ultrapure water in turn. Secondly, for constructing the graphene–AuNPs hybrid electrode, the optimal condition was as follows: 5 μL of 0.75 mg mL^{-1} graphene–AuNPs hybrid solution was dropped onto GC electrodes, and then the electrodes were left to dry in an oven desiccator and stored at 37 °C. Finally, the graphene–AuNPs hybrid electrodes were immersed in a solution containing 1 mg mL^{-1} 1-ethyl-3-(3-dimethyl-aminopropyl) carbodiimide hydrochloride (EDC) and *N*-hydroxysuccinimide (NHS) for 3 h. After rinsing with ultrapure water to get rid of the excess EDC and NHS, the activated electrodes were immersed in 50 μL of GOD (EC 1.1.3.4, 294 units mg^{-1}, from *Aspergillus niger*) solution (10 mg mL^{-1}, dissolved in 0.05 M pH 9.0 tris-HCl solution) at 4 °C for 24 h. The fabricated graphene–AuNPs–GOD hybrid electrodes were purged with ultrapure water to wipe off unbound GOD. The electrodes were stored at 4 °C when they were not in use.

3. Results and discussion

3.1 Characterization of the transformation from graphite to the graphene–AuNPs hybrid

XRD, UV-Vis, and FT-IR techniques were used to confirm the transformation from graphite to the graphene–AuNPs hybrid. In the XRD pattern (Fig. 1A), the characteristic peak of graphite (curve a) focused at 26.5° (2θ). Once the graphite was oxidized, the peak center of graphite oxide (GO) (curve b) appeared at 10.3° (2θ).[5] After being reduced by hydrazine hydrate and dispersed by ammonia, only a broad peak presented at 23.4° for graphene (curve c) was observed, which meant that most of the GO had been reduced. As for the graphene–AuNPs hybrid, the Bragg angles of 38.0°, 44.2°, 64.5° and 77.4° were clearly observed, which correspond to the (111), (200), (220) and (311) planes of the AuNPs (curve d).[17]

In addition, the FT-IR spectra of the samples were obtained in Fig. 1B, with curves a, b and c corresponding to GO, graphene and the graphene–AuNPs hybrid, respectively. As for curve a,

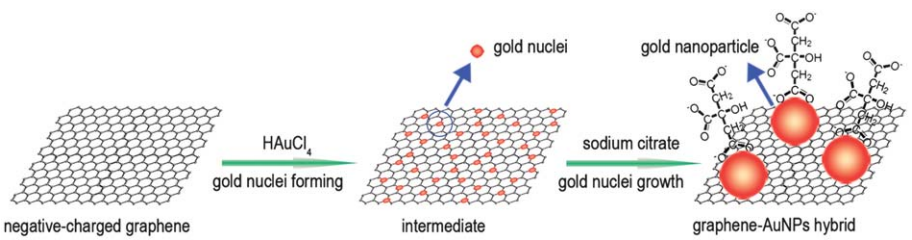

Scheme 1 Schematic diagram of synthesizing the graphene–AuNPs hybrid.

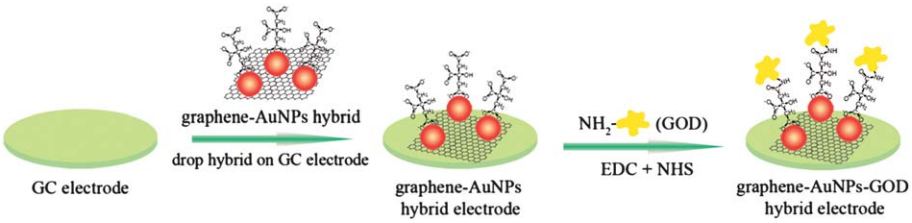

Scheme 2 Schematic diagram of fabricating the model of the amperometric glucose biosensor.

before adding hydrazine hydrate, the characteristic stretching vibration was the board peak at 3400 cm^{-1}, which was ascribed to O–H groups. The C=O stretching peak was around 1730 cm^{-1}, O–H deformation peak was at 1440 cm^{-1}, and the C–OH and C–O stretching peaks were at 1222 cm^{-1} and 1055 cm^{-1}, respectively. These results indicated that the surface of GO was functionalized with different kinds of oxygen functional groups. After the surface was reduced, the characteristic absorption of the C=O stretching peak disappeared, as shown in curve b, and the O–H stretching vibration at 3410 cm^{-1}, O–H deformation at 1398 cm^{-1} and C–O stretching at 1102 cm^{-1} were weak. These results identified that most of the oxygen functional groups had been removed.[18] Curve c in Fig. 1B showed that the absorption peak at 3400–2600 cm^{-1} became broad and distinct. It indicated the presence of $–COO^-$. The stretching peak focused at about 1670 cm^{-1} was ascribed to the C=O in $–COO^-$. In addition, the stretching peaks focused at 1402 cm^{-1} and 1090 cm^{-1} were derived from O–H and C–O stretching, respectively. All the obtained results demonstrated that the carboxyl groups in sodium citrate molecules had been attached to the AuNPs of the hybrid.

For UV-Vis absorption spectra, the maximum absorption (Fig. 1C) transferred from 231 nm of GO (curve a) to 267 nm of graphene (curve b). This transfer indicated that the electronic conjugation in the graphene sheets was refreshed.[16] The UV-Vis absorption peak at 530 nm also identified that the AuNPs had been formed on the surface of graphene, and the average size was about 30 nm (curve c).[19]

3.2 The morphology of the graphene–AuNPs hybrid and the loading amount of the AuNPs on graphene

AFM was used to identify the layer nature of the graphene. The AFM image in Fig. 2A and the statistic result in Fig. 2B showed that the thickness of graphene was about 0.6 nm, namely only two layers of single-atom-thick sheets. The morphology examined using FESEM and HRTEM was shown in Fig. 2C and Fig. 2E, respectively. In the FESEM image, it was found that AuNPs were attached to the graphene surface and scattered well on the nanosheets. It looks like the "egg-laying" of a silkworm moth on the "graphene paper". By changing the mass ratio of graphene to $HAuCl_4$ from 7 : 1 to 7 : 125, it was found that the

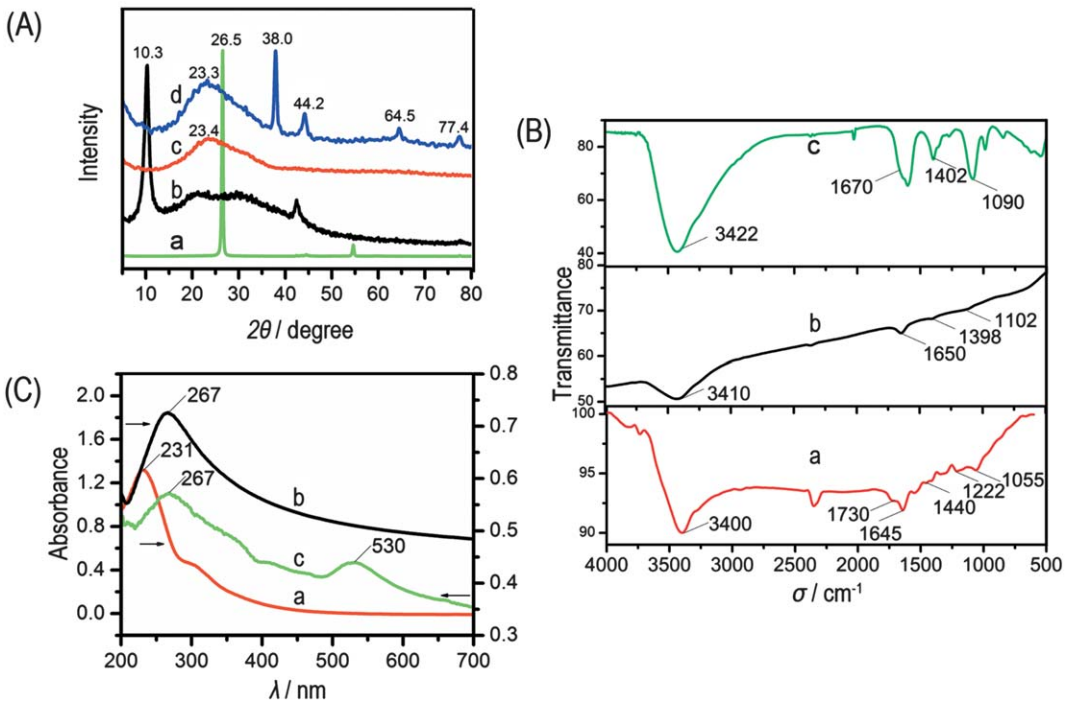

Fig. 1 (A) XRD patterns of (a) graphite, (b) GO, (c) graphene, and (d) graphene–AuNPs hybrid. (B) FT-IR spectra of (a) GO, (b) graphene, and (c) graphene–AuNPs hybrid. (C) UV-Vis absorption spectra of (a) GO, (b) graphene, and (c) graphene–AuNPs hybrid.

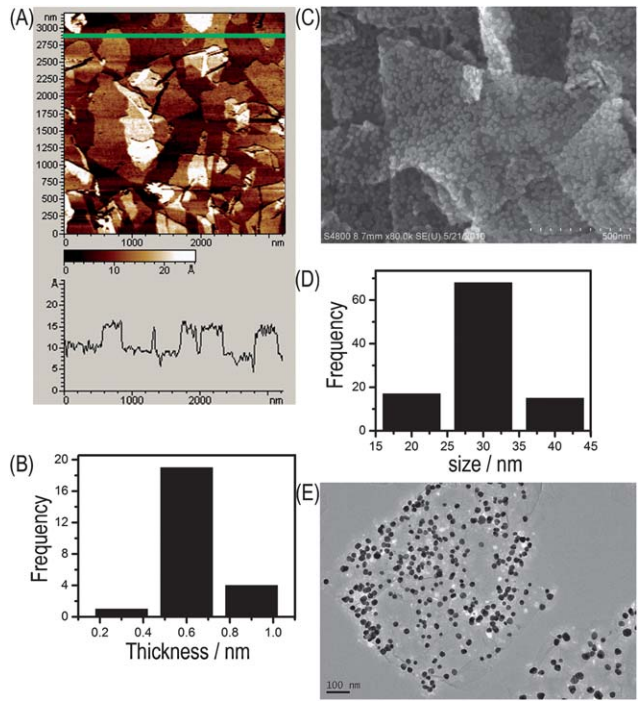

Fig. 2 (A) AFM image of graphene, cross-section analysis was based on the chosen line. (B) The histogram displaying the distribution of sheet thicknesses measured on 20 different sheets from AFM results. (C) FESEM image of the graphene–AuNPs hybrid. (D) The histogram displaying the size distributions of the AuNPs on the surface of the graphene, calculated by 100 particles from FESEM results. (E) HRTEM image of the graphene–AuNPs hybrid.

loading amount of the AuNPs on the graphene surface could be controlled. The quantity of Au in the hybrid was determined by ICP-AES technology, and the results were consistent with the stoichiometric value as shown in Table 1. It was observed that the size distribution of AuNPs on graphene changed with the different ratios of graphene to $HAuCl_4$. The optimal mass ratio of graphene to $HAuCl_4$ was 7 : 10 based on the most narrow particle size dispersion. The average size of AuNPs was about 30 nm as shown in Fig. 2D. The relative standard deviation (RSD) for the content of Au in the graphene–AuNPs hybrid was 3.33%.

It was reported that the amount of oxygen containing functional groups on the graphene surface played a key role in the linkage of AuNPs.[6a] Since almost no oxygen containing functional groups were on the graphene by the reduction of hydrazine hydrate from GO, it should be difficult to attach AuNPs on this kind of graphene surface. However, our experiments demonstrated that the oxygen containing functional groups may not be

Table 1 Comparison between the theoretical value and experimental value for the content of Au in the hybrid

m(graphene) : *m*($HAuCl_4$) (mg)	Theoretical value (%)	Experimental value (%)
7 : 1	6.42	6.01
7 : 10	40.7	42.8
7 : 125	89.6	81.4

a crucial factor for the attachment of the AuNPs. This can be explained as follows: Firstly, the negative-charged graphene bears the low reduction potential, and can adsorb and join in the reduction of Au^{3+};[6b] secondly, due to the existence of the slight excess of hydrazine hydrate in the graphene colloid solution,[16] gold nuclei could form by the assisted deoxidation;[20] thirdly, some of the carboxyl groups in the sodium citrate molecules could be attached to the AuNPs surface by a coordination bond, and the other carboxyl groups with negative charges were free, which acted as a stabilizing agent to prevent AuNPs from aggregation through electrostatic repulsion.

3.3 Direct electrochemistry of GOD bound on graphene–AuNPs electrode

The direct electrochemistry of a graphene–AuNPs–GOD hybrid electrode was studied by cyclic voltammetry. Fig. 3 displays the cyclic voltammograms (CVs) of a bare GC electrode (curve a), a graphene–AuNPs hybrid electrode (curve b), and a graphene–AuNPs–GOD hybrid electrode (curve c) in phosphate buffered saline (PBS) saturated with N_2. A couple of well-defined redox peaks with the reduction and oxidation peak potentials at −0.401 and −0.326 V respectively at the graphene–AuNPs–GOD hybrid electrode were observed. The formal potential ($E^{0'}$) was −0.364 V, which was ascribed to the characteristic peak of redox active center (flavin adenine dinucleotide, FAD) of GOD.[4b] It was demonstrated that the graphene–AuNPs hybrid could provide a favourite microenvironment for GOD to maintain its natural structure and realize its direct electrochemistry. Shan *et al.*[4b] reported that the redox peak current of GOD entrapped at the graphene electrode was about 6 μA, while curve c showed that the redox peak current was 77 μA. This phenomenon indicated that the effective loading amount of GOD on the graphene–AuNPs hybrid electrode was increased at least 10 fold. It was obviously that AuNPs played an important role in the improvement of the GOD adsorption.[4c] The homogenized AuNPs on graphene and the carboxyl groups that are present on their surface, helped more GOD molecules to bind to the hybrid electrode.

In order to evaluate the electron transfer rate, the CVs of the graphene–AuNPs–GOD hybrid electrode at different scan rates were studied. As shown in Fig. 4A, the redox peak potentials of

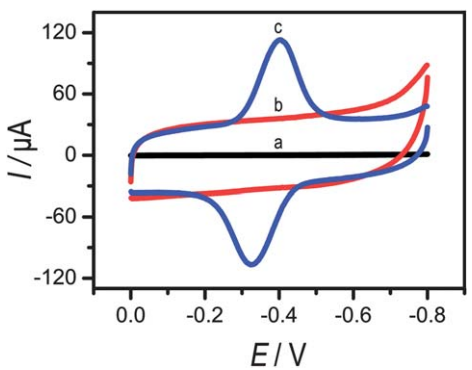

Fig. 3 CVs of (a) GC electrode, (b) graphene–AuNPs hybrid electrode, and (c) graphene–AuNPs–GOD hybrid electrode in 0.1 M PBS solution (pH 5.5) saturated with N_2 at the scan rate of 50 mV s^{-1}.

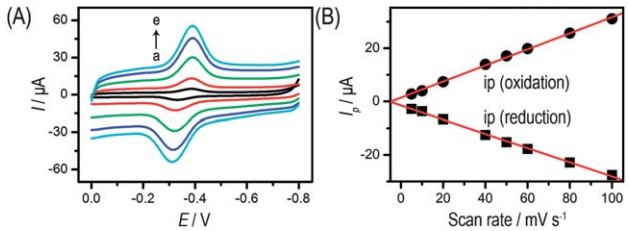

Fig. 4 (A) CVs of the graphene–AuNPs–GOD hybrid electrode at different scan rates: (a) 10 mV s^{-1}, (b) 20 mV s^{-1}, (c) 50 mV s^{-1}, (d) 80 mV s^{-1}, and (e) 100 mV s^{-1}. (B) Plot of redox peak currents *versus* various scan rates from 5 mV s^{-1} to 100 mV s^{-1}.

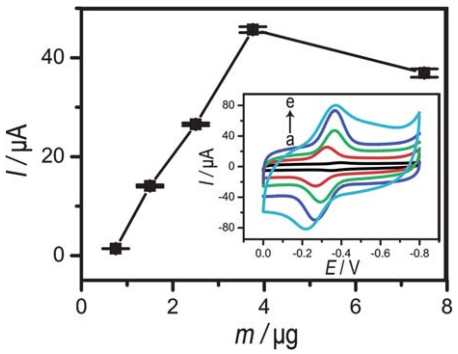

Fig. 5 The relationship between the reduction peak currents of the bound GOD and the amount of the graphene–AuNPs hybrid. Every point was an average value of four independent measurements. Inset: CVs of a series of graphene–AuNPs–GOD hybrid electrodes based on various masses of the graphene–AuNPs hybrid: (a) 0.75 μg, (b) 1.50 μg, (c) 2.50 μg, (d) 3.75 μg, and (e) 7.50 μg. These measurements were conducted in 0.1 M PBS solution (pH 5.5) saturated with N_2 at the scan rate of 50 mV s^{-1}.

GOD were unchanged with an increasing scan rate. Furthermore, Fig. 4B showed that a characteristic linear proportionality was observed between the anodic and cathodic peak currents at scan rates ranging from 10 to 100 mV s^{-1}, and the ratios of the oxidation peak current to the reduction peak current at different scan rates were close to 1. The average electron transfer number at different scan rates was estimated as 2.[22] The average half-width and peak separations were 88.7 mV and 62.7 mV, respectively, which were close to the corresponding theoretical values of 90.6 mV and 59 mV. These results indicated that the redox process of GOD was a reversible and surface-confined process. In addition, a fast electron transfer rate can be observed by small peak-to-peak separation. Based on Laviron's theory,[23] the electron transfer rate constant k_s was calculated as 7.74 ± 0.16 s^{-1}, which was much higher than that of graphene (2.83 s^{-1}),[24] graphite (1.6 s^{-1}),[25] carbon nanotubes (1.5–1.7 s^{-1}),[26] boron-doped carbon nanotubes (1.56 s^{-1}),[27] and single-walled carbon nanohorns (3.0 s^{-1}).[28] It is well known that the active redox center of GOD is protected by a protein shell, and it is difficult to realize the direct electron transfer between FAD and the electrode.[4b] However, the extraordinary electron transport property of graphene promotes the electron transfer.[4b] In addition, AuNPs provide a suitable microenvironment to maintain the activity and structure of the bound GOD. Thus it is expected that the hybrid composed of graphene and AuNPs can become a novel functional material for application in electrochemistry.

It is obvious that the graphene–AuNPs–GOD hybrid electrode current depended on its active area which was covered in the graphene–AuNPs–GOD hybrid. The active area was mainly affected by the amount of the graphene–AuNPs hybrid on the GC electrode, which controlled the binding of GOD. In order to estimate the optimal active area and the maximal current density, a series of graphene–AuNPs–GOD hybrid electrodes with various masses of the graphene–AuNPs hybrid were fabricated. The mass of the graphene–AuNPs hybrid was calculated by multiplying the volume dropped on the GC electrode and the concentration of the hybrid together. The average reduction currents of the bound GOD at all the graphene–AuNPs–GOD hybrid electrodes were calculated by four time measurements. Fig. 5 showed the relationship between the reduction peak currents of the bound GOD and the amount of the graphene–AuNPs hybrid. With an increase of the loading amount of the graphene–AuNPs hybrid from 0.75 μg to 3.75 μg, the reduction peak currents enhanced nearly linearly. However, the reduction peak currents decreased while the amount of the graphene–AuNPs hybrid was more than 3.75 μg. Therefore, 3.75 μg of the graphene–AuNPs hybrid was indicated to be the optimal condition for the construction of the graphene–AuNPs–GOD hybrid electrode to obtain the optimal active area. The calculated density of the maximal current was 171.6 μA μg^{-1} cm^{-2}. Under this condition, the RSD value of the reduction peak current in four determinations was 1.31%. These experiments indicated that the maximal current density possessed good repeatability.

3.4 Dependence of the redox potentials of GOD on solution pH

The CVs of the graphene–AuNPs–GOD hybrid electrode displayed an obvious dependence upon the pH value of the solution as shown in Fig. 6. Fig. 6A exhibited that both the cathodic and anodic peak shifted negatively with an increase in pH. A plot of $E^{0'}$ *versus* pH from 5.5 to 8.0 (curve a–c) showed a linear relationship in Fig. 6B. The linear regression equation was $E^{0'} = -0.0585\ \mathrm{pH} - 0.0469$, $R = 0.9999$. The slope was nearly equal to the expected value of 58.6 mV pH^{-1},[21] which suggested that the numbers of electrons and protons transferred in the electrochemical reaction were equal.[21]

3.5 Electrocatalysis of graphene–AuNPs–GOD hybrid electrode to reduction of dissolved O_2

The graphene–AuNPs–GOD hybrid electrode exhibited good electrocatalysis to the reduction of dissolved O_2. Fig. 7 showed

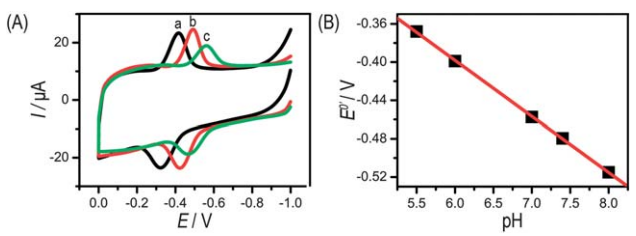

Fig. 6 (A) CVs of the graphene–AuNPs–GOD hybrid electrode in 0.1 M PBS with different pH values of (a) 5.5, (b) 7.0, and (c) 8.0 at the scan rate of 50 mV s^{-1}. (B) The relationship of $E^{0'}$ *versus* pH.

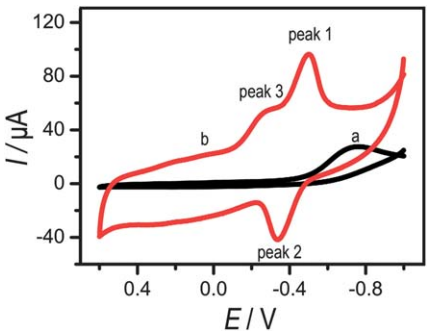

Fig. 7 CVs of (a) GC electrode and (b) graphene–AuNPs–GOD hybrid electrode in 0.1 M PBS solution (pH 5.5) saturated with O_2 at the scan rate of 50 mV s^{-1}.

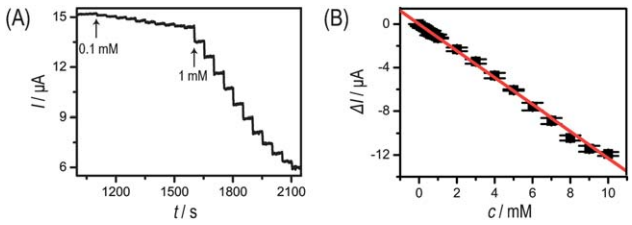

Fig. 8 (A) *I–t* curve of the model of the biosensor for successive additions of specific concentrations of glucose to 0.1 M PBS solution (pH 5.5) which was saturated with O_2. The testing solution was kept stirring. Applied potential: −0.2 V. (B) The relationship of the response current *versus* the glucose concentration. $R = 0.999$. Error bars = ± standard deviation. Every point was an average value of three model of the biosensors for independent measurements.

that at the GC electrode (curve a), the reduction potential of the dissolved O_2 in the solution was at about −0.76 V, ascribing to the diffusion of O_2 in the PBS solution. For the graphene–AuNPs–GOD hybrid electrode (curve b), peak 1 and peak 2 were ascribed to the redox peaks of FAD, while a visible reduction peak 3 could be observed at about −0.26 V. Compared to the hybrid electrode in testing solution saturated with N_2 (curve c in Fig. 3), it was obvious that peak 3 was ascribed to the reduction peak of dissolved O_2, which was much more positive than that at the GC electrode. It indicated that the reduction overpotential of dissolved O_2 was decreased for 0.5 V, therefore, the hybrid electrode exhibited good electrocatalysis to the reduction of dissolved O_2.

3.6 Determination of glucose in human serum with the model of the biosensor based on the graphene–AuNPs–GOD hybrid electrode

GOD can convert glucose into gluconolactone through reduction of the FAD, and the $FADH_2$ is reoxidized by the dissolved O_2.[29] The general reaction steps are as follows:

$$\text{GOD (FAD)} + \text{glucose} \rightarrow \text{GOD (FADH}_2\text{)} + \text{gluconolactone} \quad (1)$$

$$\text{GOD (FADH}_2\text{)} + O_2 \rightarrow \text{GOD (FAD)} + H_2O_2 \quad (2)$$

According to the reaction above, there is a linear relationship between the amount of glucose increase and the dissolved O_2 decrease. Namely, a model of the glucose amperometric biosensor could be constructed by detecting the decrease of the reduction peak current of dissolved O_2 to indicate the concentration of glucose.[4b–4d] Both the amperometric current–time (*I–t*) curve (Fig. 8) and cyclic voltammetry (Fig. 9) measurements indicated that the reduction peak current of dissolved O_2 decreased with the increase in the concentration of glucose.

Fig. 8A displays the typical amperometric response of the biosensor with successive injections of glucose to stirring PBS solution at an applied potential of −0.2 V. It was clear that the reduction current of dissolved O_2 successively decreased with the addition of glucose, and the steady-state current platform reached rapidly which indicated that the biosensor possessed the quick response to the target molecule. The linear relationship of response current *versus* the concentration of glucose was obtained as shown in Fig. 8B. The detection limit was estimated to be 35 μM at a signal/noise (S/N) of 3, and the linear range of glucose concentration was from 0.1 mM to 10 mM. When the concentration of glucose was higher than 10 mM, a plateau was observed, which showed the characteristics of the Michaelis–Menten kinetics. The apparent Michaelis–Menten constant (*K*) provides an indication of the enzyme–substrate kinetics, and *K* is generally used to evaluate the biological activity of the immobilized enzyme. According to the Lineweaver–Burk equation, *K* was estimated to be 4.73 mM, which was smaller than 10.73 mM of GOD on AuNPs–platinum nanoparticles/multiwall carbon nanotubes.[30a] The smaller value of *K* showed that the bound GOD on the graphene–AuNPs hybrid electrode obtained higher enzymatic activity.[30] In order to characterize the repeatability, three model of the biosensors were independently fabricated by the same way for measurement. The RSD value of the results determined at a glucose concentration of 5 mM (the middle point of the linear range of glucose concentrations) was 0.74%.

The model of the glucose biosensor can be used to determine the level of blood sugar concentration in a human serum sample utilizing a standard addition method. As shown in Fig. 9A, Cyclic voltammetry was performed at the model of the glucose biosensor in a standard human serum sample. The electrocatalytic peak current of dissolved O_2 decreased linearly upon increasing the glucose concentration. The calibration curve of the response current *versus* the glucose concentration in a standard human serum sample was shown in Fig. 9B. The detection limit

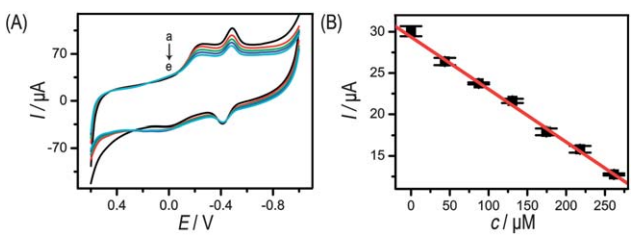

Fig. 9 (A) CVs of the model of the biosensor in standard human serum sample solutions containing (a) 0 μM, (b) 87.2 μM, (c) 130.8 μM, (d) 174.4 μM, and (e) 218 μM glucose. (B) The calibration curve of the response currents *versus* the glucose concentrations in standard human serum sample. $R = 0.998$. Error bars = ± standard deviation. Every point was an average value of three model of the biosensors for independent measurements.

Table 2 Determination of the glucose in human serum samples by the model of the biosensor

Sample (No.)	Determined values[a] (mM)	Referenced values[b] (mM)	Relative deviations (%)
1	18.13	17.51	3.5
2	8.31	8.28	0.36
3	5.20	5.36	−3.1
4	10.01	9.77	2.5
5	6.01	6.16	−3.8
6	7.76	7.34	5.8

[a] Values determined by the model of the biosensor. [b] Values provided by Nanjing University hospital.

was estimated to be 8.9 μM at an S/N of 3, and the linear range of blood sugar concentration was from 43.6 μM to 261.6 μM. The RSD value of three electrodes by cyclic voltammetry from the three model of the biosensors determined at a blood sugar concentration of 130.8 μM (the middle point of the linear range of blood sugar concentrations) was 1.19%. The practical clinical analysis was based on six different kinds of human serum samples. The analysis results were shown in Table 2. The results were in good agreement with the values provided by the Nanjing University hospital, and the average relative deviation was 3.2% for six successive measurements. The interference of other molecules in the samples for determination of the glucose was not found. Fig. 9B showed the sensitivity of the biosensor was 64 μA mM^{-1}, which was more than 100 folds larger than that of ref. 4*c* (0.55 μA mM^{-1}). Compared to the model of the biosensor reported by Wang *et al.*,[4d] our model of the biosensor was improved, which can mainly be ascribed to the graphene–AuNPs hybrid. Firstly, due to the predominate conductivity, AuNPs could facilitate electron transfer between the immobilized GOD and the electrode. Secondly, because the AuNPs obtained the unique properties to provide a suitable microenvironment for GOD immobilization retaining its biological activity, the activity of GOD could be maintained for more than 4 months. Thirdly, due to the homogenized AuNPs on graphene, more GOD molecules could bind to the hybrid electrode. Compared to the sensitivity (0.15 μA mM^{-1}) reported by Wang *et al.*, the value 64 μA mM^{-1} in the present work was increased at least 400 fold.

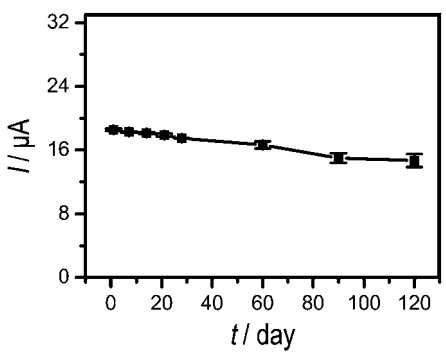

Fig. 10 The relationship of the reduction peak currents of the GOD bound and the time for storage. Error bars = ± standard deviation. Every point was an average value of the three model of the biosensors for independent measurements.

There was a direct correlation between the stability of the model of the biosensor and the activity of GOD bound on the graphene–AuNPs–GOD hybrid electrode. The activity of GOD could be demonstrated by the redox peak currents of the bound GOD at the graphene–AuNPs–GOD hybrid electrode. In order to characterize the stability and repeatability, the three model of the biosensors were independently fabricated by the same way for measuring the changes of the reduction peak currents during the storage. Fig. 10 showed the average reduction peak current of the three model of the biosensors retained 80% of the initial signal after they were stored at 4 °C for four months, and the maximum RSD value of the reduction peak currents was 5.6% (120 days). It demonstrated that the model of the biosensor obtained good stability and repeatability, and it is a promising candidate to determine the concentration of glucose in practical clinical analysis.

4 Conclusions

In summary, the graphene–AuNPs hybrid was synthesized *in situ* by introducing AuNPs to the graphene with negative charge. The loading amount of AuNPs can be controlled, and the AuNPs can be scattered well on the nanosheets. Due to the carboxyl groups on the surface of the AuNPs, GOD molecules were covalently bound to the hybrid electrode and the direct and reversible electron transfer between GOD and the electrode was observed. The blood sugar concentration in human serum samples was tested by the novel model of the glucose biosensor, and the results were consistent with the measurements performed in the Nanjing University hospital.

Acknowledgements

We gratefully appreciate the National Natural Science Foundation (20975048, 20821063), the National Basic Research Program (2011CB933502) of China, and the International S&T Cooperation Projects of China (2010DFA42060).

References

1 K. S. Novoselov, A. K. Geim, S. V. Morozov, D. Jiang, Y. Zhang, S. V. Dubonos, I. V. Grigorieva and A. A. Firsov, *Science*, 2004, **306**, 666–669.
2 R. F. Service, *Science*, 2008, **322**, 1785–1785.
3 J. R. Miller, R. A. Outlaw and B. C. Holloway, *Science*, 2010, **329**, 1637–1639.
4 (*a*) Y. C. Si and E. T. Samulski, *Chem. Mater.*, 2008, **20**, 6792–6797; (*b*) C. S. Shan, H. F. Yang, J. F. Song, D. X. Han, A. Ivaska and L. Niu, *Anal. Chem.*, 2009, **81**, 2378–2382; (*c*) C. S. Shan, H. F. Yang, D. X. Han, Q. X. Zhang, A. Ivaska and L. Niu, *Biosens. Bioelectron.*, 2010, **25**, 1070–1074; (*d*) Z. J. Wang, X. Z. Zhou, J. Zhang, F. Boey and H. Zhang, *J. Phys. Chem. C*, 2009, **113**, 14071–14075.
5 Y. X. Xu, H. Bai, G. W. Lu, C. Li and G. Q. Shi, *J. Am. Chem. Soc.*, 2008, **130**, 5856–5857.
6 (*a*) G. Goncalves, P. Marques, C. M. Granadeiro, H. I. S. Nogueira, M. K. Singh and J. Gracio, *Chem. Mater.*, 2009, **21**, 4796–4802; (*b*) B. S. Kong, J. X. Geng and H. T. Jung, *Chem. Commun.*, 2009, (16), 2174–2176; (*c*) J. B. Liu, S. H. Fu, B. Yuan, Y. L. Li and Z. X. Deng, *J. Am. Chem. Soc.*, 2010, **132**, 7279–7281; (*d*) F. Liu, J. Y. Choi and T. S. Seo, *Chem. Commun.*, 2010, **46**, 2844–2846; (*e*) R. Muszynski, B. Seger and P. V. Kamat, *J. Phys. Chem. C*, 2008, **112**, 5263–5266; (*f*) W. J. Hong, H. Bai, Y. X. Xu, Z. Y. Yao, Z. Z. Gu and G. Q. Shi, *J. Phys. Chem. C*, 2010, **114**, 1822–1826; (*g*) Y. X. Fang, S. J. Guo, C. Z. Zhu, Y. M. Zhai and E. K. Wang,

Langmuir, 2010, **26**, 11277–11282; (*h*) Y. K. Kim, H. K. Na and D. H. Min, *Langmuir*, 2010, **26**, 13065–13070.
7 S. J. Guo, D. Wen, Y. M. Zhai, S. J. Dong and E. K. Wang, *ACS Nano*, 2010, **4**, 3959–3968.
8 R. S. Sundaram, C. Gomez-Navarro, K. Balasubramanian, M. Burghard and K. Kern, *Adv. Mater.*, 2008, **20**, 3050–3053.
9 S. M. Paek, E. Yoo and I. Honma, *Nano Lett.*, 2009, **9**, 72–75.
10 G. Williams, B. Seger and P. V. Kamat, *ACS Nano*, 2008, **2**, 1487–1491.
11 V. C. Tung, L. M. Chen, M. J. Allen, J. K. Wassei, K. Nelson, R. B. Kaner and Y. Yang, *Nano Lett.*, 2009, **9**, 1949–1955.
12 L. Bahshi, M. Frasconi, R. Tel-Vered, O. Yehezkeli and I. Willner, *Anal. Chem.*, 2008, **80**, 8253–8259.
13 G. S. Lai, F. Yan and H. X. Ju, *Anal. Chem.*, 2009, **81**, 9730–9736.
14 A. W. Zhu, Y. Tian, H. Q. Liu and Y. P. Luo, *Biomaterials*, 2009, **30**, 3183–3188.
15 U. H. F. Bunz and V. M. Rotello, *Angew. Chem., Int. Ed.*, 2010, **49**, 3268–3279.
16 D. Li, M. B. Muller, S. Gilje, R. B. Kaner and G. G. Wallace, *Nat. Nanotechnol.*, 2008, **3**, 101–105.
17 R. J. Cui, C. Liu, J. M. Shen, D. Gao, J. J. Zhu and H. Y. Chen, *Adv. Funct. Mater.*, 2008, **18**, 2197–2204.
18 Y. Si and E. T. Samulski, *Nano Lett.*, 2008, **8**, 1679–1682.
19 W. Haiss, N. T. K. Thanh, J. Aveyard and D. G. Fernig, *Anal. Chem.*, 2007, **79**, 4215–4221.
20 K. Jasuja and V. Berry, *ACS Nano*, 2009, **3**, 2358–2366.
21 X. Shangguan, H. F. Zhang and J. B. Zheng, *Electrochem. Commun.*, 2008, **10**, 1140–1143.
22 E. Laviron, *J. Electroanal. Chem.*, 1979, **100**, 263–270.
23 E. Laviron, *J. Electroanal. Chem.*, 1979, **101**, 19–28.
24 X. H. Kang, J. Wang, H. Wu, I. A. Aksay, J. Liu and Y. H. Lin, *Biosens. Bioelectron.*, 2009, **25**, 901–905.
25 Q. J. Chi, J. D. Zhang, S. J. Dong and E. K. Wang, *Electrochim. Acta*, 1994, **39**, 2431–2438.
26 C. X. Cai and J. Chen, *Anal. Biochem.*, 2004, **332**, 75–83.
27 C. Y. Deng, J. H. Chen, X. L. Chen, C. H. Mao, L. H. Nie and S. Z. Yao, *Biosens. Bioelectron.*, 2008, **23**, 1272–1277.
28 X. Q. Liu, L. H. Shi, W. X. Niu, H. J. Li and G. B. Xu, *Biosens. Bioelectron.*, 2008, **23**, 1887–1890.
29 (*a*) S. Q. Liu and H. X. Ju, *Biosens. Bioelectron.*, 2003, **19**, 177–183; (*b*) H. Yoon, S. Ko and J. Jang, *J. Phys. Chem. B*, 2008, **112**, 9992–9997.
30 (*a*) X. Chu, D. X. Duan, G. L. Shen and R. Q. Yu, *Talanta*, 2007, **71**, 2040–2047; (*b*) X. H. Kang, Z. B. Mai, X. Y. Zou, P. X. Cai and J. Y. Mo, *Anal. Biochem.*, 2007, **369**, 71–79; (*c*) Y. J. Zou, C. L. Xiang, L. X. Sun and F. Xu, *Biosens. Bioelectron.*, 2008, **23**, 1010–1016.